J. Vis. Commun. Image R. 42 (2017) 173–182

Contents lists available at ScienceDirect

J. Vis. Commun. Image R.

journal homepage: www.elsevier.com/locate/jvci

Satellite image classification using Genetic Algorithm trained radial basis function neural network, application to the detection of flooded areas ☆

Akansha Singh [a,*], Krishna Kant Singh [b]

[a] The NorthCap University, Gurgaon, India
[b] Dronacharya College of Engineering, Gurgaon, India

ARTICLE INFO

Article history:
Received 24 October 2016
Revised 14 November 2016
Accepted 25 November 2016
Available online 29 November 2016

Keywords:
Radial basis function
Genetic Algorithm
Landsat 8
Classification
Change detection

ABSTRACT

In this paper, a semi supervised method for classification of satellite images based on Genetic Algorithm (GA) and Radial Basis Function Neural Network (RBFNN) is proposed. Satellite image classification problem has two major concerns to be addressed. The first issue is mixed pixel problem and the second issue is handling large amount of data present in these images. RBFNN function is an efficient network with a large set of tunable parameters. This network is able to generalize the results and is immune to noise. A RBFNN has learning ability and can appropriately react to unseen data. This makes the network a good choice for satellite images. The efficiency of RBFNN is greatly influenced by the learning algorithm and seed point selection. Therefore, in this paper spectral indices are used for seed selection and GA is used to train the network. The proposed method is used to classify the Landsat 8 OLI images of Dongting Lake in South China. The application of this method is shown for detection of flooded area over this region. The performance of the proposed method was analyzed and compared with three existing methods and the error matrix was computed to test the performance of the method. The method yields high producer's accuracy, consumer's accuracy and kappa coefficient value which indicated that the proposed classifier is highly effective and efficient.

1. Introduction

Classifying remote sensing images is a tedious and complex task as it involves a number of factors to be considered. Designing an efficient classification method is influenced by the user's needs, the spatial resolution of the remotely sensed data, compatibility with previous work, available image-processing and classification algorithms, and time constraints. Also the classification system should be informative, exhaustive, and separable [1,2]. Satellite image classification is preceded by a number of preprocessing tasks like noise removal, image segmentation for feature extraction, contrast enhancement [3]. The selection of appropriate number and type of training samples is also very important for image classification [1]. Selection of training samples for remote sensing images is very complicated since the images are heterogeneous and contain mixed pixels, i.e., pixels belonging to more than one type of class. Therefore selection of training data must be done based on ground reference data, spatial resolution and complexity of the scene in the image. Before developing any classification system it is important to select the correct type of remote sensing data as different sensors provide images with different spatial, radiometric, spectral, and temporal resolutions. A variety of advanced classification methods based on artificial neural networks, decision trees, fuzzy sets, neuro-fuzzy techniques, and expert systems are used for image classification [4]. Artificial neural networks have been applied in image classification problem as the classification problem can be specified in the form of finding suitable nonlinear mathematical fitting for function approximation. These methods can be broadly categorized as supervised, unsupervised, parametric versus non parametric, hard versus soft classification, per-pixel, sub pixel and per field classification [5]. Neural network based classifiers are being widely used due to several advantages like they are easily adaptable to various types of data and inputs, they overcome the problem of mixed pixel by giving fuzzy output and are used with multiple images [6,7]. A number of unsupervised classifiers based on fuzzy techniques are available in the literature. Most popularly used fuzzy clustering algorithm is Fuzzy C- Means [10]. It optimizes the value of an objective function but the disad-

☆ This paper has been recommended for acceptance by Zicheng Liu.

* Corresponding author.
E-mail address: akanshasing@gmail.com (A. Singh).

http://dx.doi.org/10.1016/j.jvcir.2016.11.017
1047-3203/

vantage of this method is that it gets stuck at local optima. an improvement of FCM is IFP-FCM, which assigns crisp membership degrees but is less sensitive to noise[9]. Fuzzy Local Information C-Means Clustering (FLICM) introduces a fuzzy factor which improves the clustering results as well as makes the algorithm insensitive to noise [10]. Among the various kinds of neural networks currently under active research, RBF networks attract extensive research interest. A variety of approaches for training radial

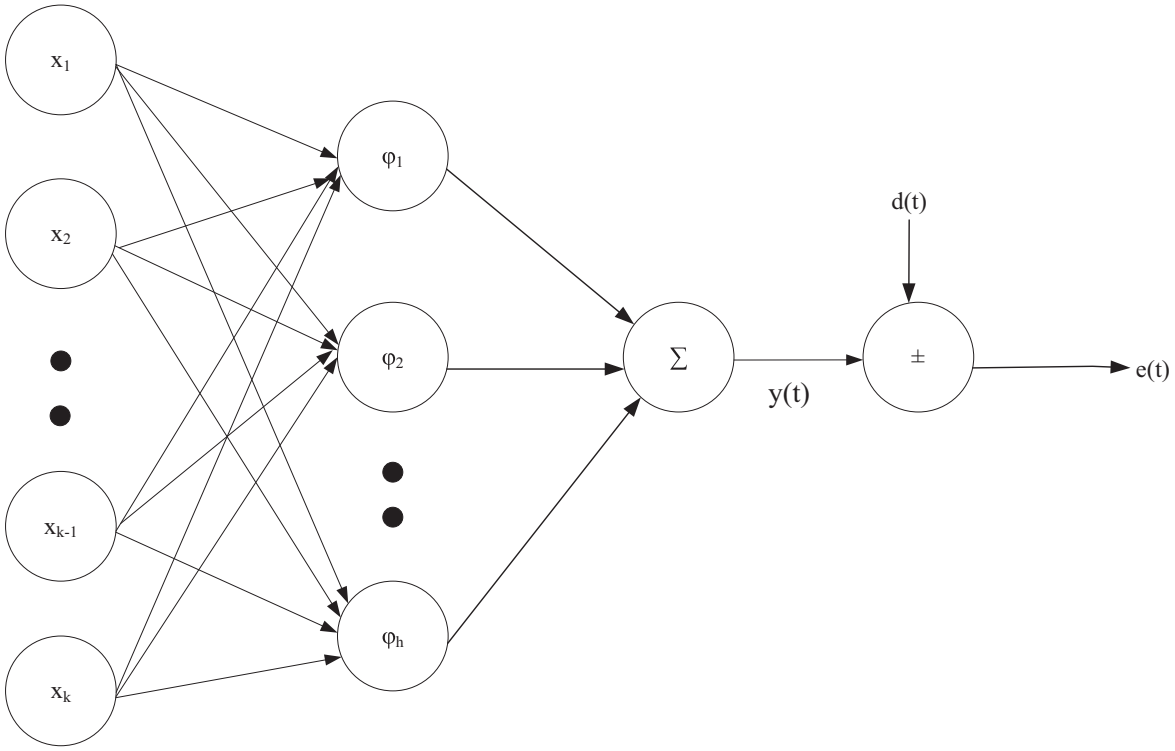

Fig. 1. Structure of RBFNN.

Fig. 2. Location map and areas affected by floods [21].

basis function networks have been developed [11]. The available training methods pose a serious threat of getting stuck at the local minima. Genetic Algorithms work on a population instead of a single point in the search space, they can climb many peak in parallel and thus reduce the chances of finding local minima [12]. Remote sensing image classification is applied to various areas like urban planning, disaster management, vegetation monitoring, and forest cover monitoring. One of the most significant areas is monitoring of natural disasters. Natural disasters are serious events which end up from earth's natural processes [6]. They cause tremendous threat to life and property, the amount of losses is proportional to the vulnerability of the affected space [7]. The occurrence of natural disasters in the recent years has increased greatly. The major disasters include tsunamis, floods, volcanic eruptions, and earthquakes etc. Floods are one of the most frequent and devastating natural hazards that occur worldwide. Flood occurs due to excessive rainfall in a short duration of time and consequent high river discharge causes large amount of damage. Flooding results in huge economic losses, destruction of ecological resources, food shortages and starvation of million people. Thus one of the major concerns of various countries is to monitor flooding so as to reduce the effect of floods. In the era of satellites, remote sensing data is used effectively for assessment, identification and management of flood disaster [13]. The application of satellite imagery for flood mapping began with the use of Landsat Thematic Mapper and Multispectral Scanner, the Satellite Pour l'Observation de la Terre [14], the Advanced Very High Resolution Radiometer [15], the Advanced Spaceborne Thermal Emission and Reflection Radiometer (ASTER), MODIS, and Landsat-7 sensors [16]. The pre and post flood Landsat 7 TM images were used to identify water and non-water features to identify flooded areas [17]. Flooded areas and damaged buildings due to the 2011 Japan tsunami were identified based on the difference of backscattering coefficients from the pre and post tsunami TerraSAR-X intensity images [18]. A recent method identifies flooded area in Kashmir region using hybrid Kohonen Fuzzy C-Means sigma classifier [19].

In this paper, an image classification method based on GA trained RBFNN for remotely sensed images are proposed. The proposed method uses RBFNN to find the optimal centres for different land cover classes. Radial basis function network provides a way to handle the large amount of data present in remote sensing images. The efficiency of RBFNN is greatly influenced by the initial seed selection and training used. Thus to enhance the efficiency of RBFNN spectral

Table 1
Band characteristics of Landsat 8 OLI.

Bands	Wavelength (μm)	Resolution (m)
Band 1 – Coastal aerosol	0.43–0.45	30
Band 2 – Blue	0.45–0.51	30
Band 3 – Green	0.53–0.59	30
Band 4 – Red	0.64–0.67	30
Band 5 – Near Infrared (NIR)	0.85–0.88	30
Band 6 – SWIR 1	1.57–1.65	30
Band 7 – SWIR 2	2.11–2.29	30

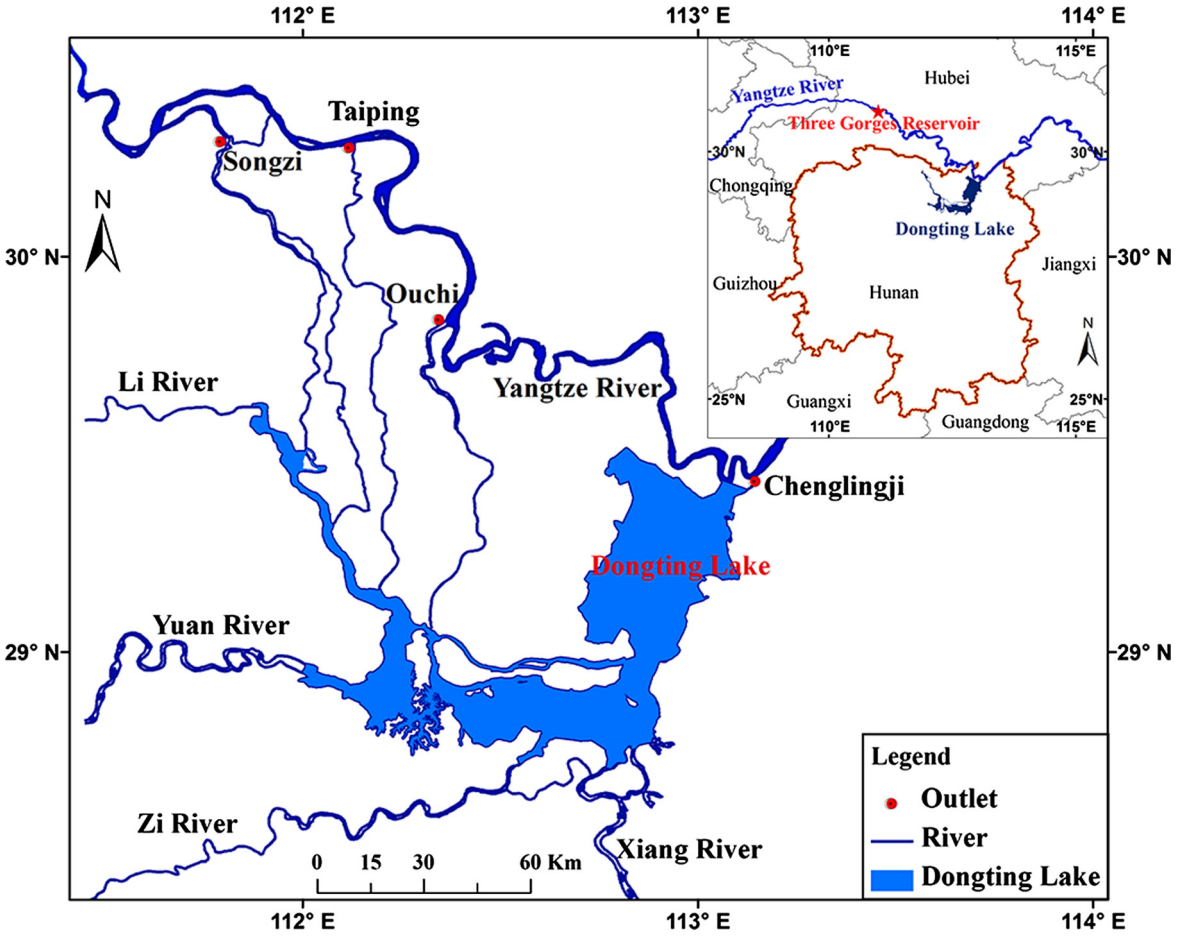

Fig. 3. Location map [22].

indices and training based on GA is used in this work. GA has proved to be one of the most powerful optimization tools in a large space and hence work effectively in finding cluster centres for image classification. The training of RBFNN with GA gives a powerful and efficient method for remote sensing image classification. Landsat 8 OLI images of South China area are classified using the proposed method. The method is applied to detect the flooded area near Dongting lake in South China. In June 2016, heavy rainfall occurred in South China area which caused disastrous flooding all over the area causing devastation. The study area comprises of area of Dongting Lake in Yangtze River Basin of South China. Pre and post Landsat 8 OLI flooding images are classified using GA trained RBFNN into different land cover classes. Post classification comparison is then applied on the pre and post classified images to identify the change in water class indicating flooded areas.

2. Radial basis function neural network

A radial basis function neural network is a feed forward network comprising of three layers namely input layer, hidden layer and output layer. The input layer connects the external environment with the network and the output layer gives the output of the network. The hidden layer incorporates the specialized activation functions called radial basis function (RBF). These functions produce localized, bounded, and radially symmetric activations that decreases the distance from the function's centres. Each node in the hidden layer represents a RBF that is centred on a vector in the feature space. The k dimensional input vector χ is fed to each of the j^{th} radial basis hidden units. Each unit of the hidden layer is a radial centre denoted by $c_1, c_2, \ldots, c_h$. Fig. 1 shows the structure of the RBFNN.

Thus the output of the j[th] hidden unit is given by:

$$\varphi_j = \varphi(\|\chi - c_j\|) = \exp\left(-\frac{\|\chi - c_j\|^2}{2\sigma_j^2}\right) \quad (1)$$

where the input vector $\chi^T = \{x_1, x_2, \ldots, x_N\}$, $\|\ \|$ is the Euclidean distance between the input and the j_{th} centre, $\varphi(.)$ is the RBF function and σ_j is the standard deviation of the j_{th} Gaussian function. It can be computed using Eq. (2)

$$\sigma = d_{max}/\sqrt{h} \quad (2)$$

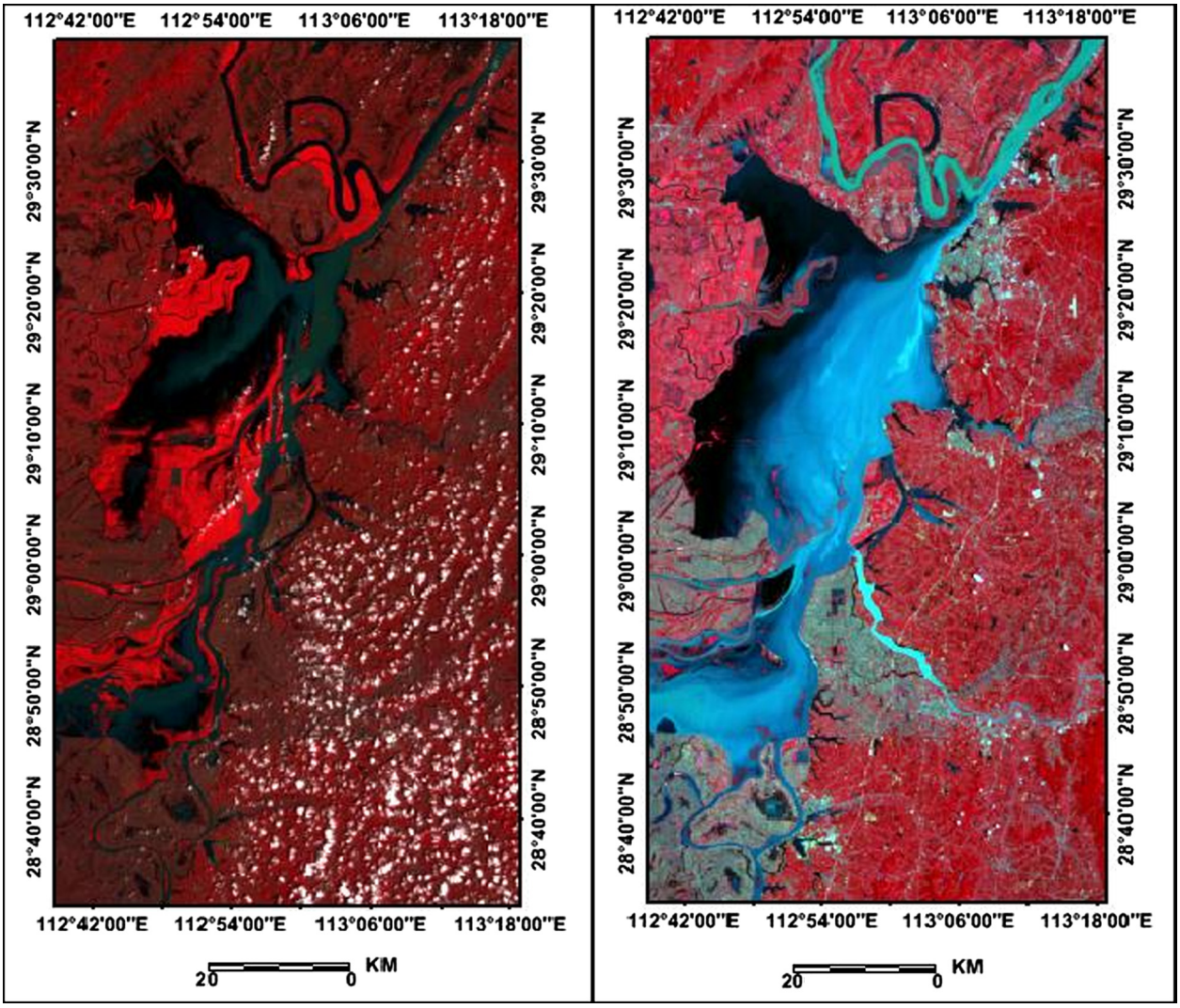

Fig. 4. False natural color composite (R: SWIR, G: NIR, B: Green) Pre and Post flooding Landsat 8 Operational Land Imager (OLI) images acquired on (a) 27th March 2016 (b) 28th July 2016 respectively [23]. (For interpretation of the references to color in this figure legend, the reader is referred to the web version of this article.)

where d_{max} is the maximum distance between the centres. The output y of the network is given by,

$$y = \sum_{j=1}^{h} w_j \cdot \varphi(\|\chi - c_j\|) \tag{3}$$

where w_j is the weight of the j^{th} hidden unit and h is the number of centres. The weights of RBF are obtained by network training.

3. Training using Genetic Algorithm

Genetic Algorithm is a randomized search and optimization technique guided by the principle of natural genetic systems [20]. The RBFNN is trained using GA as follows:

Step 1. Population Initialization: The GA starts with a group of chromosomes known as the population. Chromosomes correspond to the array of variable values to be optimized. Thus, the h hidden nodes represent a chromosome and thee radial centres are initialized to random values. A chromosome is now represented as

$$C = [c_1, c_2, c_3, \ldots, c_h] \tag{4}$$

The population has N_{pop} chromosomes and is a $N_{pop} \times N_{bits}$ matrix filled with random values.

Step 2. Fitness Computation: The fitness value of each of the N_{pop} chromosomes is evaluated as the response of applying the radial basis function. The basis function used in this paper is the least square error. This is given as follows:

$$\xi(t) = \frac{1}{2}(d(t) - y(t))^2 \tag{5}$$

where $d(t)$ is the desired output obtained from the training set and $y(t)$ is the output obtained from the network on the test data.

Step 3. Selection: The N_{pop} chromosomes are arranged in descending order based on the value of the fitness function. Only the best chromosomes are kept while others are discarded. The surviving population is denoted by N_{keep} from which two parents are selected to generate off springs. In this paper, weighted rank is used for selection of parents. This is a probabilistic approach in which the probability of a chromosome is computed from the rank, n, of a chromosome as follows:

$$P_n = \frac{N_{keep} - n + 1}{\sum_{n=1}^{N_{keep}} n} \tag{6}$$

Two top chromosomes with highest probabilities are selected for mating.

Step 4. Mutation: This is a genetic operator that is used to combine information to generate new off springs. A crossover rate is decided based on which the two parents combine information to generate new off springs.

Step 5. Step 2–4 are iterated while the termination condition is met.

4. Site description and satellite data used

In Yangtze River Basin, China, heavy rainfall in South China began on 14 June 2016. The area was severely affected by the heavy rains and about 2.8 million from eleven provinces were affected [21]. About 600,000 people were affected and almost 240,000 people had to move nearby places. Fig. 2 shows the areas affected by flooding.

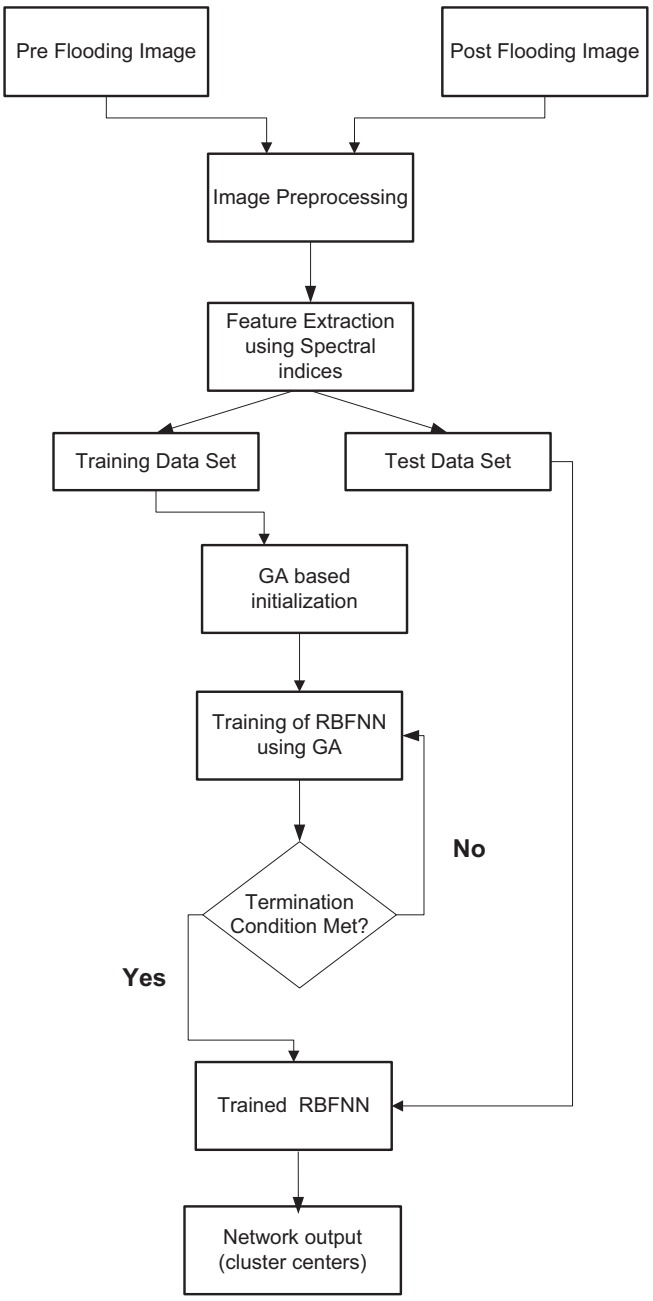

Fig. 5. Flowchart of the proposed method.

Pre and Post flooding Landsat 8 Operational Land Imager (OLI) images acquired on 27th March 2016 and 28th July 2016 respectively have been used for the study. The Operational Land Imager (OLI), has 11 bands with 30 m multi-spectral spatial resolutions along a 185 km (115 miles) wide swath, covering wide areas of the Earth's landscape while providing sufficient resolution to distinguish features like urban centres, farms, forests and other land uses. The band characteristics of Landsat 8 are given Table 1.

Fig. 3 shows the location map of the study area. The Dongting Lake located at 28°42′–29°38′N and 111°52′–113°08′E lies in the

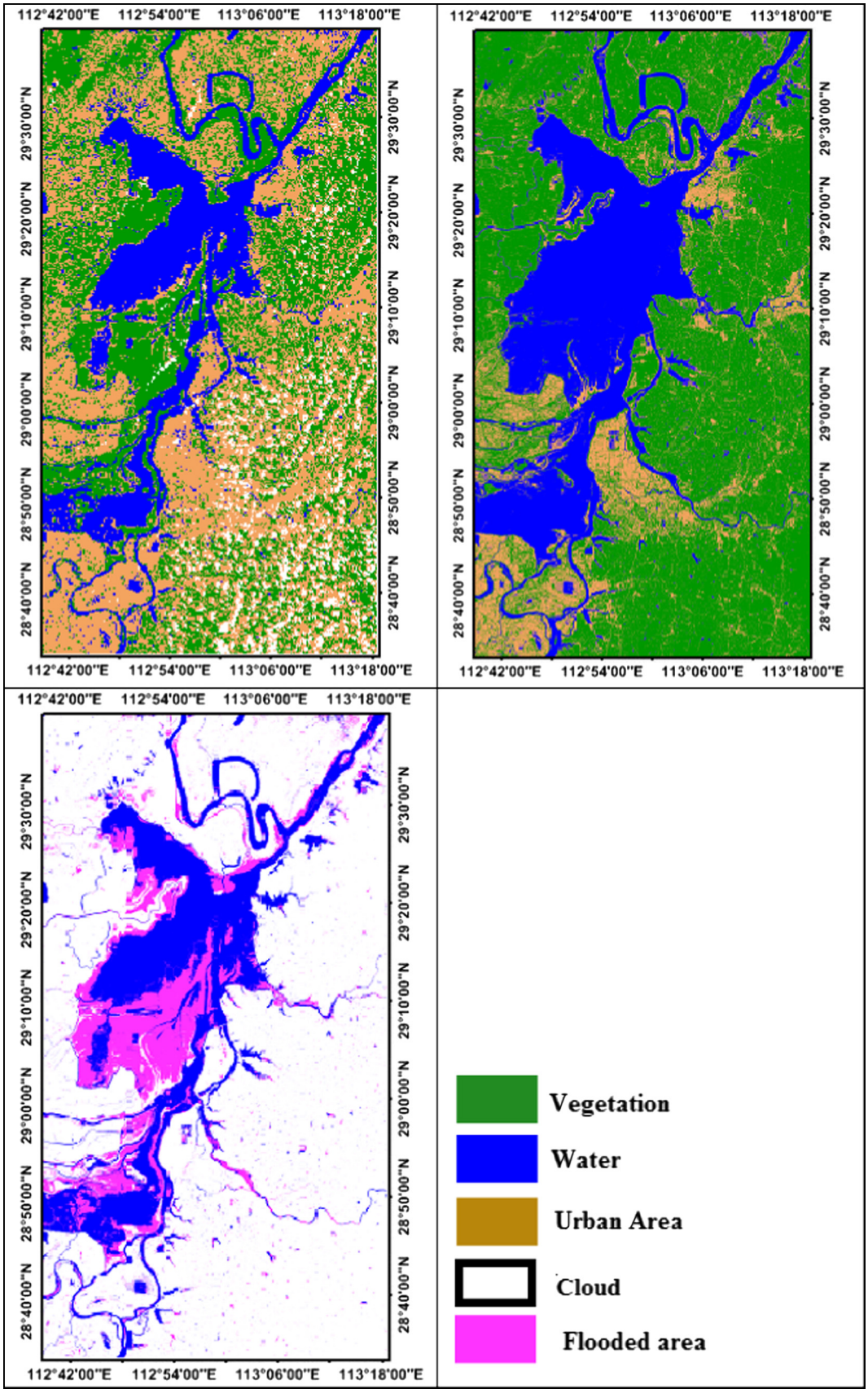

Fig. 6. (a) Pre flooding classified image. (b) Post flooding classified image. (c) Classified change map.

north of Hunan Province. The lake spans over an area of 2794.7 km^2 and is the second largest freshwater lake in China.

The Dongting Lake experiences great seasonal variations in water levels because it is affected by the monsoon climate. The annual mean lowest water level is only 20.19 m, which often happens in January. By contrast, the annual mean highest water level can reach 30.24 m, which usually occurs in July [22]. The false color composite of a subset of pre and post flooding images covering areas of Dongting Lake is shown in Fig. 4.

5. Methodology

The flow chart of the proposed method is shown in Fig. 5. These steps are as follows:

5.1. Image preprocessing

Quantative comparison of multi-temporal images requires conversion of DN values to reflectance. The conversion is done to overcome the brightness difference due to image acquisition under different sun illumination conditions should be compensated. Secondly, the difference in DN values due to the seasonal adjustment of sensor parameters by the data provider. Thus, the DN values are converted into the top of atmosphere reflectance ($\boldsymbol{\rho_{TOA}}$) to resolve the abovementioned issues.

5.2. Feature extraction using spectral indices

Spectral indices are band ratios that are used to highlight a particular land cover type. A number of spectral indices are available in the literature [24]. In this paper, Normalized Difference Vegetation Index (NDVI), Normalized Difference Water Index (NDWI), Normalized Difference Built up Index (NDBI) and first component of Principal component Analysis (PC-1) is used. NDVI is used to highlight vegetated areas using visible and near infrared bands. Dense vegetation absorbs visible light and reflects near infrared light whereas sparse vegetation reflects visible light and absorbs near infrared light. The NDVI image is computed using the following Eq. (7)

$$NDVI = \frac{\psi_{nir} - \psi_{red}}{\psi_{nir} + \psi_{red}} \tag{7}$$

NDWI is used to highlight the water bodies and snow covered areas in satellite imageries. NDWI makes use of green and NIR band of the electromagnetic spectrum to highlight water. Water features have positive values of NDWI whereas vegetation and soil have NDWI values equal to or less than zero.

Table 2
Confusion Matrix for pre flooding image.

Reference Data	Water	Vegetation	Urban	Cloud	Total
Water	**40**	1	1	0	42
Vegetation	2	**87**	2	0	91
Urban	2	2	**103**	2	109
Cloud	0	0	1	**13**	14
Total	44	90	107	15	**256**

Table 3
Accuracy Results for pre flooding image.

Class name	Producers Accuracy	User's Accuracy	Conditional Kappa
Water	90.91	95.24	0.9425
Vegetation	96.67	95.60	0.9322
Urban	96.26	94.50	0.9054
Cloud	86.67	92.86	0.9241
Overall Accuracy: 94.92% Overall Kappa: 0.9237			

Table 4
Confusion Matrix for post flooding image.

Reference Data	Water	Vegetation	Urban	Cloud	Total
Water	**64**	1	1	0	66
Vegetation	3	**138**	2	0	143
Urban	1	2	**44**	0	47
Cloud	0	0	0	0	0
Total	68	141	47	0	**256**

Table 5
Accuracy Results for post flooding image.

Class name	Producers Accuracy	User's Accuracy	Conditional Kappa
Water	94.12	96.97	0.9587
Vegetation	97.87	96.50	0.9222
Urban	93.62	93.62	0.9218
Cloud	–	–	–
Overall Accuracy: 96.09% Overall Kappa:0.9338			

$$NDWI = \frac{\psi_{green} - \psi_{nir}}{\psi_{green} + \psi_{nir}} \quad (8)$$

NDBI is used for highlighting the built up areas and barren land have high increase in reflectance values from MIR band to NIR band. The speed at which the increase in reflectance value occurs is greater than any other land cover type.

$$NDBI = \frac{\psi_{mir} - \psi_{nir}}{\psi_{mir} + \psi_{nir}} \quad (9)$$

where $\psi_{nir}, \psi_{red}, \psi_{mir}, \psi_{green}$ represent the near infrared, red, mid infrared and green band respectively.

The mean value of the spectral indices are used for seed selection of the RBFNN. The mean values of NDVI, NDWI, NDBI and PC-1 are used for vegetation, water, built up area and cloud classes.

5.3. Image classification using GA trained RBF neural network

The proposed method finds optimal cluster centres for classification of the satellite images. The method comprises of the following steps:

5.3.1. Initialization

The network is initialized with the following values. The network is built with h hidden nodes. The weights are initialized randomly with a uniform distribution around 0 and with an empirical variance set at 0.02.

5.3.2. Centre computation

The centres are computed using GA trained RBFNN. The h hidden nodes correspond to the h cluster centres of the h classes. The training of the network is performed as discussed in section.

5.3.3. Termination condition

The network termination is one of the most important steps. If the network termination criteria is not properly set then overfitting might occur. This will lead to divergence. The total objective function of the network is given in Eq. (10)

$$E_t(q) = \sum_{t=1}^{T}\sum_{h=1}^{H}\xi_r(t) \quad (10)$$

Table 6
Confusion Matrices of different methods for Pre Flooding image.

Method	Classes	Water	Vegetation	Urban	Cloud
FCM	Water	**39**	2	1	0
	Vegetation	2	**85**	4	0
	Urban	1	6	**100**	2
	Cloud	0	0	1	**13**
IFP-FCM	Water	**39**	2	1	0
	Vegetation	2	**86**	3	0
	Urban	2	4	**102**	1
	Cloud	0	0	1	**13**
FLICM	Water	**39**	2	1	0
	Vegetation	2	**87**	2	0
	Urban	2	3	**103**	1
	Cloud	0	0	1	**13**

Table 7
Confusion Matrices of different methods for Post Flooding image.

Method	Classes	Water	Vegetation	Urban
FCM	Water	**62**	3	1
	Vegetation	4	**135**	4
	Urban	1	5	**41**
IFP-FCM	Water	**63**	2	1
	Vegetation	3	**136**	4
	Urban	1	4	**42**
FLICM	Water	**63**	2	1
	Vegetation	3	**137**	3
	Urban	1	4	**42**

Table 8
Accuracy and kappa.

Image	Method	Overall Accuracy	Kappa
Pre Flooding	FCM	92.58	0.8883
	IFP-FCM	93.75	0.9058
	FLICM	94.53	0.9176
	GA trained RBF	94.92	0.9237
Post Flooding	FCM	92.97	0.8803
	IFP-FCM	94.14	0.9005
	FLICM	94.53	0.9069
	GA trained RBF	96.09	0.9338

t: index of training, T: total iterations, h: output of the h_{th} layer, q: index of training patterns and $\xi_r(t)$ is the cost function given in Eq. (5).

The termination criteria is given in Eq. (11). If the condition is met the network stops else the iteration count is incremented one and next iteration is started.

$$\frac{E_t(q+1)-E_t(q)}{E_t(q+2)-E_t(q+1)} < \epsilon \tag{11}$$

The value of ϵ is generally chosen between 0.5 and 1.

6. Results

The proposed network is implemented in Matlab R2013a and the results can be accelerated by parallel processing on many-core processor [25,26]. The pre and post flooding images given in Fig. 4 are classified into four classes namely vegetation, water, urban area, clouds as shown in Fig. 6(a) and (b). Post classification comparison method is applied on the pre and post classified images to obtain a classified change map which highlights the flooded area. The result of change detection is shown in Fig. 6(c). For p classes a total of $p*(p-1)$ change classes are possible. The pre and post images are classified into four classes, thus total twelve change classes are possible. But since the aim is to detect flooded areas thus all those change classes in which any class is changed to water class are merged into one class and named as flooded area class which shows the flooded areas. The scene under consideration covers an area of 796.7411 sq km. The original water bodies spanned over an area of 131.9548 sq km and after flooding this area increased to 214.9548 sq. km. Thus, the total flooded area is approximately 83 sq. km.

The performance evaluation of the proposed classifier is done using accuracy assessment of the classifier. It gives an insight of the detected change results. One of commonly used methods is to apply an error matrix which can be used to compute a number of assessment elements like overall accuracy and kappa coefficient [27]. One of the most important task in accuracy assessment is selection of sampling strategy for collection of ground points. The commonly used approach is to use the training pixels that are used to train the classifier for accuracy assessment. But the limitation with this approach is that the training pixels are not random and also they are influenced by the analyst's knowledge about the location of different classes. An alternative to this is random selection of points but when points are selected randomly certain small classes are ignored. Thus, stratified random technique is used as it is not biased and also the selection of points is random covering all classes. In this paper, stratified random technique from ERDAS™ software is used for accuracy assessment. The images are classified in Matlab R2013a and thus the geotiffwrite function of Matlab R2013a, which writes a georeferenced image is used. The results are analyzed using confusion matrices and the overall accuracy, kappa coefficient, producer's accuracy and user's accuracy is computed. The reference points are chosen in an unbiased manner using stratified random sampling. Tables 2–5 shows the various assessment elements for both pre and post flooding images. The overall accuracy is 94.92% and 96.09% for pre and post flooding images respectively. The value of kappa coefficient is 0.9237 for pre flooding and 0.9338 for post flooding image. The proposed method was compared with three other methods FCM [8], IFP-FCM [9] and FLICM [10]. The results are shown in Tables 6–8.

7. Conclusion

This paper presents a novel image classification method for satellite images. A GA trained RBFNN is proposed here, the seed selection is done using spectral indices like NDVI, NDBI, NDWI and PC-1. The proposed method trains the radial basis function network with Genetic Algorithm and thus combines the advantages of both. The RBFNN provides easy design, good generalization, strong tolerance to input noise, and online learning ability. The neural network handles the large amount of data present in satellite images. The use of GA makes the search optimal as it is a powerful optimization tool and works well when the search space is large as in satellite images. The method is applied on Landsat 8 Operational Land Imager (OLI) covering Dongting Lake, South China area. The multispectral images are classified into four classes using the proposed method implemented in MatlabR2013a. These classified images are used to detect the flooded area over the region. The results obtained are compared with other existing state of the art methods and it is observed that the proposed method gives better results.

References

[1] D.A. Landgrebe, Signal Theory Methods in Multispectral Remote Sensing, Wiley, Hoboken, NJ, 2003, 508.
[2] A. Singh, K.K. Singh, Z. Ren, Change detection from remotely sensed images based on a decision theoretic method, in: Proc. of Computing for Sustainable Global Development (INDIACom), 2015, 2015, pp. 495–498.
[3] Z. Ji, Y. Huang, Q. Sun, G. Cao, A spatially constrained generative asymmetric Gaussian mixture model for image segmentation, J. Vis. Commun. Image Represent. 40 (2016) 611–626.
[4] K.K. Singh, M.J. Nigam, K. Pal, A. Mehrotra, A fuzzy kohonen local information C-means clustering for remote sensing imagery, IETE Tech. Rev. 31 (1) (2014) 75–81.
[5] D. Lu, Q. Weng, A survey of image classification methods and techniques for improving classification performance, Int. J. Remote Sens. 28 (5) (2007) 823–870.
[6] K.K. Singh, A. Singh, Detection of 2011 Sikkim earthquake-induced landslides using neuro-fuzzy classifier and digital elevation model, Nat. Hazards 83 (2) (2016) 1027–1044.
[7] A. Mehrotra, K.K. Singh, M.J. Nigam, K. Pal, Detection of tsunami-induced changes using generalized improved fuzzy radial basis function neural network, Nat. Hazards 77 (1) (2015) 367–381.
[8] J.C. Bezdek, Pattern Recognition with Fuzzy Objective Function Algorithms, Plenum Press, New York, 1981.
[9] F. Höppner, F. Klawonn, Improved fuzzy partitions for fuzzy regression models, Int. J. Approx. Reason. 32 (2) (2003) 85–102.
[10] S. Kirindis, V. Chatzis, A robust fuzzy local information c means clustering algorithm, IEEE Trans. Image Process. 19 (5) (2010) 1328–1337.
[11] G.W. Chang, C.I. Chen, Y.F. Teng, Radial-basis-function-based neural network for harmonic detection, IEEE Trans. Ind. Electron. 57 (6) (2010) 2171–2179.
[12] S.A. Billings, G.L. Zheng, Radial basis function network configuration using genetic algorithms, Neural Networks 8 (6) (1995) 877–890.
[13] B. Pradhan, M. Shafie, Flood hazard assessment for cloud prone rainy areas in a typical tropical environment, Disaster Adv. 2 (2) (2009) 7–15.
[14] J.P. Watson, A visual interpretation of a LANDSAT mosaic of the Okavango-delta and surrounding area, Remote Sens. Environ. 35 (1) (1991) 1–9.
[15] G. Stancalie, A. Diamandi, C. Corbus, S. Catana, Application of EO data in flood fore-casting for the Crisuri Basin, Romania, Flood Risk Management: Hazards, Vulnerability and Mitigation Measures, Springer-Verlag, New York, 2004.
[16] Y. Wang, J.D. Colby, K.A. Mulcahy, An efficient method for mapping flood extent in a coastal floodplain using Landsat TM and DEM data, Int. J. Remote Sens. 23 (18) (2008) 3681–3696.
[17] N. Mori, T. Takahashi, T. Yasuda, H. Yanagisawa, Survey of 2011 Tohoku earthquake tsunami inundation and run-up, Geophys. Res. Lett. 38 (7) (2011).
[18] R. Hoque, D. Nakayama, H. Matsuyama, J. Matsumoto, Flood monitoring, mapping and assessing capabilities using RADARSAT remote sensing, GIS and ground data for Bangladesh, Nat. Hazards 57 (2) (2011) 525–548.
[19] K.K. Singh, A. Singh, Identification of flooded area from satellite images using Hybrid Kohonen Fuzzy C-Means sigma classifier, Egypt. J. Remote Sens Space Sci. (2016), http://dx.doi.org/10.1016/j.ejrs.2016.04.003.
[20] K.K. Singh, A. Mehrotra, M.J. Nigam, K. Pal, Unsupervised change detection from remote sensing images using hybrid genetic FCM, in: Proc. of 2013 Students Conference on Engineering and Systems (SCES), 2013, pp. 1–5.
[21] Available : <http://floodlist.com/asia/china-july-2016-floods-cost-33-billion-dollars> (accessed 15 September 2016).
[22] Y. Hu, J. Huang, Y. Du, P. Han, W. Huang, Monitoring spatial and temporal dynamics of flood regimes and their relation to wetland landscape patterns in Dongting Lake from MODIS time-series imagery, Remote Sens. 7 (6) (2015) 7494–7520.
[23] USGS Available: <http://earthexplorer.usgs.gov>.

[24] K.K. Singh, M.J. Nigam, K. Pal, Detection of 2011 Tohoku tsunami inundated areas in Ishinomaki City using generalized improved fuzzy Kohonen clustering network, Eur. J. Remote Sens. 47 (2014) 461–475.
[25] C. Yan, Y. Zhang, J. Xu, F. Dai, L. Li, Q. Dai, F. Wu, A highly parallel framework for HEVC coding unit partitioning tree decision on many-core processors, IEEE Signal Process. Lett. 21 (5) (2014) 573–576.
[26] C. Yan, Y. Zhang, J. Xu, F. Dai, J. Zhang, Q. Dai, F. Wu, Efficient parallel framework for HEVC motion estimation on many-core processors, IEEE Trans. Circuits Syst. Video Technol. 24 (12) (2014) 2077–2089.
[27] R.G. Congalton, K. Green, Assessing the Accuracy of Remotely Sensed Data: Principles and Practices, CRC, Boca Raton, 2008.